energies

MDPI

Article

Fault Classification System for Switchgear CBM from an Ultrasound Analysis Technique Using Extreme Learning Machine

Sanuri Ishak [1], Chong Tak Yaw [2,*], Siaw Paw Koh [2,*], Sieh Kiong Tiong [2], Chai Phing Chen [1] and Talal Yusaf [3,*]

[1] Department of Electrical and Electronics Engineering, Universiti Tenaga Nasional (The Energy University), Jalan IKRAM-UNITEN, Kajang 43000, Malaysia; sanuri@lion.com.my (S.I.); chencp@uniten.edu.my (C.P.C.)
[2] Institute of Sustainable Energy, Universiti Tenaga Nasional (The Energy University), Jalan IKRAM-UNITEN, Kajang 43000, Malaysia; siehkiong@uniten.edu.my
[3] School of Engineering and Technology, Central Queensland University, Brisbane, QLD 4009, Australia
* Correspondence: chongty@uniten.edu.my (C.T.Y.); johnnykoh@uniten.edu.my (S.P.K.); t.yusaf@cqu.edu.au (T.Y.)

Abstract: Currently, the existing condition-based maintenance (CBM) diagnostic test practices for ultrasound require the tester to interpret test results manually. Different testers may give different opinions or interpretations of the detected ultrasound. It leads to wrong interpretation due to depending on tester experience. Furthermore, there is no commercially available product to standardize the interpretation of the ultrasound data. Therefore, the objective is the correct interpretation of an ultrasound, which is one of the CBM methods for medium switchgears, by using an artificial neural network (ANN), to give more accurate results when assessing their condition. Information and test results from various switchgears were gathered in order to develop the classification and severity of the corona, surface discharge, and arcing inside of the switchgear. The ultrasound data were segregated based on their defects found during maintenance. In total, 314 cases of normal, 160 cases of the corona, 149 cases of tracking, and 203 cases of arcing were collected. Noise from ultrasound data was removed before uploading it as a training process to the ANN engine, which used the extreme learning machine (ELM) model. The developed AI-based switchgear faults classification system was designed and incorporated with the feature of scalability and can be tested and replicated for other switchgear conditions. A customized graphical user interface (GUI), Ultrasound Analyzer System (UAS), was also developed, to enable users to obtain the switchgear condition or classification output via a graphical interface screen. Hence, accurate decision-making based on this analysis can be made to prioritize the urgency for the remedial works.

Keywords: artificial neural network; condition-based maintenance; decision-making; extreme learning machine; fault diagnosis; graphical user interface; switchgear; ultrasound

Citation: Ishak, S.; Yaw, C.T.; Koh, S.P.; Tiong, S.K.; Chen, C.P.; Yusaf, T. Fault Classification System for Switchgear CBM from an Ultrasound Analysis Technique Using Extreme Learning Machine. *Energies* **2021**, *14*, 6279. https://doi.org/10.3390/en14196279

Academic Editor: Djaffar Ould-Abdeslam

Received: 26 July 2021
Accepted: 27 September 2021
Published: 2 October 2021

1. Introduction

Many switchgear failures are caused by gradual degradation [1,2] of the devices, such as the insulators [3–7], switches [8–13], and connectors [14–20]. At the preliminary stage, these electrical faults, as shown in Figure 1, can produce noises that are detectable in the frequency range (20 kilohertz (kHz) to 100 kHz) by an ultrasonic detection system [21,22]. Hence, an ultrasonic inspection system can be used appropriately to ensure electrical faults are detected early enough to prevent catastrophic or unexpected failure. An ultrasonic detection system allows the inspectors to instantly hear the generated signal that undoubtedly cannot be ordinarily seen [23–26].

The common electrical faults of the switchgear are the corona [27–34], tracking [27,35], and arcing [34,36–38], as shown in Figure 1. Furthermore, the switchgear might be experiencing more than one specific fault at the same time. The corona activity can be sufficiently

advanced to the tracking stage on an insulation board resting on a bus. The likely consequence of the specific fault, is that carbon deposits and a light brown discoloration of the insulation board possibly will be noticed by the maintenance personnel. The undetected corona can typically lead to further deterioration of the insulator and lead to tracking and eventually arcing.

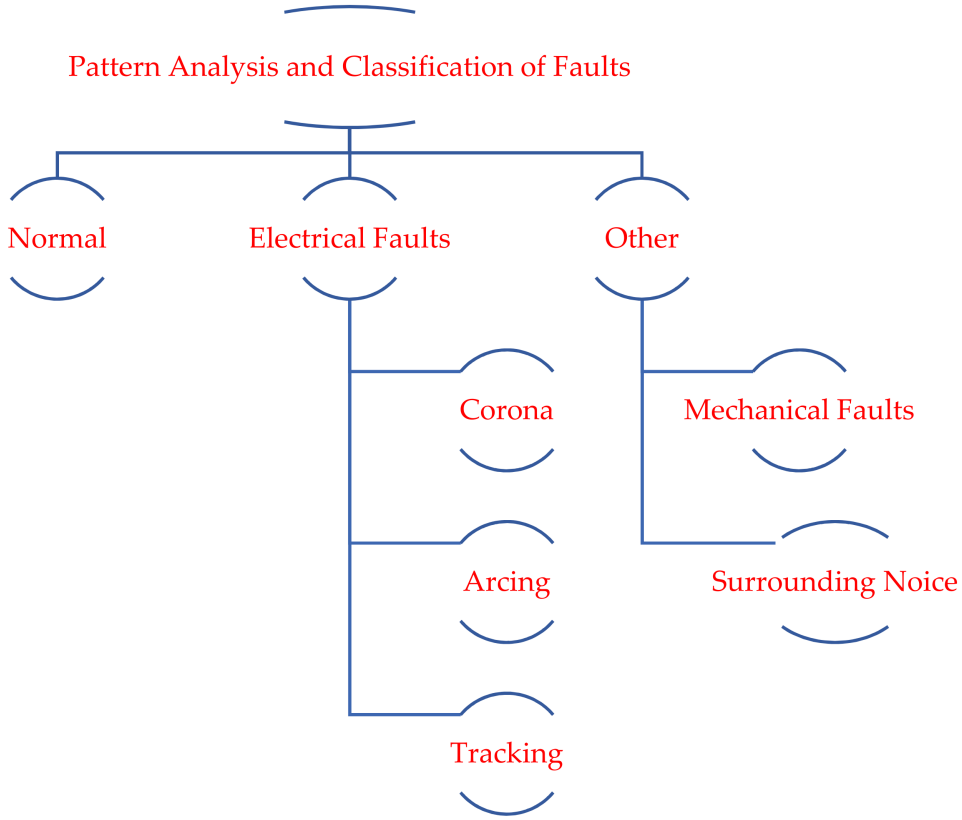

Figure 1. The mechanical and electrical faults of the switchgear.

The principal concept of condition-based maintenance (CBM) is to use equipment deterioration information extracted and featured from sensing and data processing to minimize the downtime of the system by prognostics and diagnostics [39–43]. To do so, a CBM framework for machinery equipment consists of several key steps (data acquisition, data pre-processing, feature extraction, health assessment, prognostic, and diagnostic). In other words, CBM is a maintenance procedure where maintenance operations are conducted on the existing assets. The state of the asset is examined via performance data (often collected by various instruments or/and sensors), tests, and visual inspections. The collected data can be analyzed to know the condition of the equipment such that the maintenance can be executed before failure.

The focus in this article is on the CBM method by using the airborne ultrasound test (AUT) for a medium voltage (MV) switchgear. Figure 2 is the testing equipment for AUT. Airborne ultrasound is used to identify the surface partial discharge (PD). In short, PD is an inadequate electrical failure among conductors. In addition, the corona is a type of PD, where it is happening on the surface of the conductor because of the ionization of air. Corona can be produced without current flow and reveals voltage problems. The major dictating factor for its presence is a high potential in the electrical field.

Figure 2. Airborne ultrasonic test equipment.

Machine learning has been widely applied for various purposes in switchgear systems for fault diagnosis [30,44–55] as well as prediction [56–58] and maintenance [44]. To be precise, the focus of machine learning is based on neural networks [46,47,50–52,54,56], support vector machine (SVM) [45,49], and extreme learning machine (ELM) [30], and have been widely used in switchgear system fault diagnosis. Literature studies state that by using extreme learning machine (ELM) the learning speed can be instantly quicker than conventional feed-forward neural network (FFNN) learning algorithms, while also achieving improved generalization performance [59–65]. It was able to come up with a universal approximation using random biases and input weights. Hidden neurons were not needed in this case; instead, the weights needed to learn about the link between the output and hidden layers. In addition, ELM tends to reach the smallest training error but also the smallest norm of considerable weights [66–72]. Therefore, the proposed learning algorithm undoubtedly tends to have a more precise, good generalization performance for FFNNs [63,64,67,70,72,73]. Intrinsically, ELM has been selected as an artificial intelligence tool for this article.

The objective of this article is to develop ELM classification models for detecting and classifying various types of switchgear faults. In addition, The ELM model for switchgear faults identification is able to provide accurate switchgear fault classification in both the time domain and in the frequency domain after the training and validation process. Lastly, a graphical user interface (GUI) is developed to enable users to obtain the switchgear condition or classification. The article is categorized as follows. In Section 2, the methods are presented. In Section 3, the data collection for switchgear's fault is explained. Section 4 discusses the expert rule to enhance the accuracy of the classification output of this article. Section 5 provides the results and the discussion. The proposed GUI for detecting switchgear's fault is shown in Section 6. Finally, Section 7 concludes the article.

2. Methods

The key focus is switchgear health condition identification via potential faults classification with an AI tool. Electrical fault and mechanical fault ultrasound data in ultrasound audio format were carefully analyzed to accurately determine the specific types of faults. In Figure 3 is shown the flow chart diagram of the digital signal processing (DSP) and ELM for the faults classification system.

Raw distribution data were gathered from the power utility company (PUC) from seven states in Peninsular Malaysia, namely, Kedah, Kuala Lumpur, Melaka, Selangor, Perak, Negeri Sembilan, and Johor. The MATLAB program read each data/input up to 10,000 bits. The program was set to read for the first 10,000 bits. If the data were less than 10,000 bits, the program read all the data. The data that were more than 10,000 bits were not analyzed.

In this stage, the AI was developed by using ELM for ultrasound fault classification since it is the most suitable for this research. MATLAB software was used to facilitate the programming for ELM. In order for the sound to be processed by MATLAB, the raw data were converted into a matrix format for the plotting and manipulation process. This was done by using the function "wavread". Visual Basic (VB) software was utilized to make the software more user friendly by interacting via a graphical user interface (GUI).

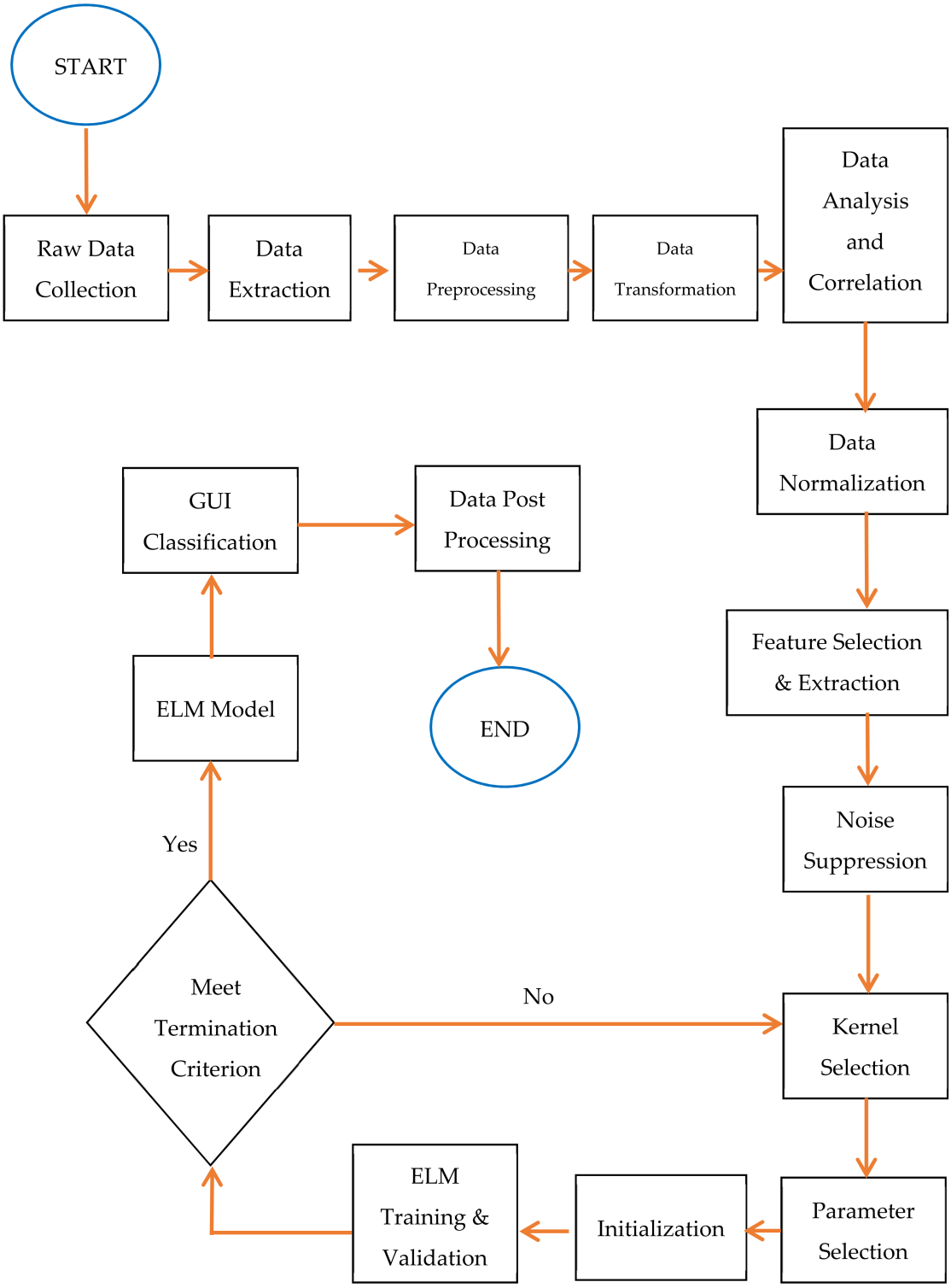

Figure 3. Flowchart diagram of the research method.

In this article, raw data were collected from the test results obtained by using AUT equipment. The ultrasound data were recorded using the file format audio layer-3 (known as *mp3*), moving picture experts group (MPEG), or waveform audio (known as *wav*). Data transformation is a data pre-processing technique that transforms or consolidates the data into a format that is more appropriate for a specific machine learning algorithm. The data, which were in the *wav* and *mp3* file formats, were converted into a matrix format to suit the MATLAB software criteria.

The data analysis and correlation process is to determine the sampling rate of the data and to choose the best baseline for the sampling rate. Based on the data gathered, it was decided that 11,025 bits is the baseline. If the data have two or more sampling rates, it underwent a process called data normalization to get a mutual relationship or link with others.

Normalization basically is like doing scaling in data transformation, but only that the data normalization scaling is done on the "individual sample to the unit norm". Normalization also represented the minimum and maximum values (0, 1) and was applied to the input. The program was designed to enable identifying the waveform based on the time domain and frequency domain in feature selection and extraction. In noise suppression, the system will eliminate the first 1000 bits of data to cut unnecessary noise due to interference during the test equipment setup.

The kernel is to help us do certain calculations faster, which otherwise would involve computations in higher-dimensional space. Kernel methods are for pattern analysis in machine learning. The general task of pattern analysis is to find and study general types of relations (principal components, rankings, clusters, classifications, and correlations) in datasets. The kernel's trick in simplest form is to transform the data into another dimension that has a clear separating margin between the classes of data. In this article, ELM was selected as a kernel because it only uses one hidden layer and give a fast result.

A few parameters were defined to be feed into the single hidden layer in the ELM system, such as the number of nodes and data amplitude range for the time domain and frequency domain. The first value for the parameters is to be keyed into the coding, starting from a small value of the node and the amplitude range in the initialization process.

Some data were used to simulate for training to check the consistency of the output. The training data were used to simulate the parameters in ELM. The activation function was initialized, which started from a small value. Data were keyed into the programming to get the desired output and compared to the actual output.

2.1. Meet Termination Criterion

A decision was made at this stage whether the result is accepted or not based on the criteria. The accepted criteria were 85% and above. If the accuracy was more than 85%, the system executed the termination, from where it went to the next stage of the program; i.e., the ELM model. If the accuracy did not meet the criteria, which was less than 85%, the program went back to the kernel selection process, where the user needs to reconsider the whole processor and may have to look into the value of the parameter initialized and repeat the whole process until the criterion is met.

2.2. ELM Model

Once the criteria were met as mentioned above, the parameters, namely, weight, amount of hidden layer nodes, and value of each node in the hidden layer, were saved and remembered in the ELM model.

2.2.1. Training Phase

PD Detector was used to collect the data. Input data, X is shown in Equation (1), based on the concept of ELM.

$$X = \begin{bmatrix} x_{11} & x_{12} & \cdots & x_{1M} \\ x_{21} & \cdots & \cdots & \cdots \\ \cdots & \cdots & \cdots & \cdots \\ x_{N1} & \cdots & \cdots & x_{NM} \end{bmatrix}_{N \times M} \quad (1)$$

M is the number of hidden neurons and set to 10,000 and number of data samples N, yielding Equation (2).

$$X = \begin{bmatrix} X_{11} & X_{12} & \cdots & X_{110,000} \\ X_{21} & X_{22} & \cdots & X_{210,000} \\ \vdots & \vdots & \ddots & \vdots \\ X_{N1} & X_{N2} & \cdots & X_{N10,000} \end{bmatrix}_{N \times 10,000} \tag{2}$$

The target output vector, T, is shown in Equation (3).

$$T = \begin{bmatrix} t_1 \\ t_2 \\ \vdots \\ t_N \end{bmatrix} \tag{3}$$

The next step was initialization. The number of activation functions was defined to be a positive numeric value. The common choice for the activation function was the gaussian sigmoid activation function or radial basis function (RBF). Therefore, the activation function is applied into the hidden layer where the activation function is the sigmoid activation function and RBF, shown in Equations (4) and (5), respectively. Assign the bias, b, and the input weight matrix, a, randomly.

$$H_1 = \frac{1}{1 + e^{-(a_i . x_j^T + b_i)}} \tag{4}$$

$$H_1 = e^{\{-b_i ||x_j, -, a_i||^2\}} \tag{5}$$

In addition, all nodes were applied with the sigmoid and RBF functions. Then, the hidden layer matrix was computed using Equation (6).

$$Hidden\ Layer = \begin{bmatrix} H_1 \\ H_2 \\ \vdots \\ H_N \end{bmatrix}_{N \times L} \tag{6}$$

The activation function in this article was chosen for the programming of the classifier, which is the sigmoid function, where L is the number of neurons in the hidden layer.

The output weight matrix, W, is equal to $H^{-1}\ Y$. Unfortunately, the inverse matrix cannot be solved because H is probably a non-symmetry matrix. Therefore, a Moore–Penrose pseudo inverse matrix method was employed to evade this problem using Equation (7).

$$W = (H^T\ H)^{-1}\ H^T\ Y \tag{7}$$

where Y is the targeted output.

Use the same training data to calculate the accuracy rate after the W is computed. Equation (8) was used to compute the output matrix, $Y = (y_1\ y_2 \ldots\ y_N)^T$.

$$Y = signum(HW) \tag{8}$$

$$signum(v) = \begin{cases} 1 & if\ v \geq 0 \\ -1 & else \end{cases} \tag{9}$$

The formula to calculate the accuracy rate of training data is shown in Equation (10).

$$Accuracy\ Rate = \left(\frac{Number\ of\ training\ data\ that\ coreectly\ classified}{Number\ of\ training\ data,\quad N} \times 100\% \right) \tag{10}$$

The final step was to save *L*, *a*, *b*, and W for the validation and prediction phases.

2.2.2. Validation Phase

Respective target output vector, $\boldsymbol{D}$, and input vector, $\boldsymbol{W}$, with the training pairs with *P* validation samples were collected, as shown in Equation (11).

$$\boldsymbol{W} = \begin{bmatrix} w_{11} & w_{12} & \dots & w_{1M} \\ w_{21} & \dots & \dots & \dots \\ \dots & & & \\ \dots & \dots & \dots & \dots \\ w_{P1} & \dots & \dots & w_{PM} \end{bmatrix}_{P \times M}$$

$$\boldsymbol{D} = \begin{bmatrix} d_1 \\ d_2 \\ \dots \\ d_P \end{bmatrix}_{P \times 1} \tag{11}$$

L, *a*, *b*, and *W* were loaded from a previous phase.

The calculation for hidden layer matrix, $\boldsymbol{H}$, with a sigmoid activation function, is defined in Equations (12) and (13), respectively.

$$\boldsymbol{H} = \begin{bmatrix} G(\mathbf{a}_1, b_1, \mathbf{w}_1) & \dots & G(\mathbf{a}_L, b_L, \mathbf{w}_1) \\ \vdots & \dots & \vdots \\ G(\mathbf{a}_1, b_1, \mathbf{w}_P) & \dots & G(\mathbf{a}_L, b_L, \mathbf{w}_P) \end{bmatrix}_{P \times L} \tag{12}$$

$$G(\mathbf{a}_i, b_i, \mathbf{w}_j) = \frac{1}{1 + \exp(-(\mathbf{a}_i \cdot \mathbf{w}_j^T + b_i))} \tag{13}$$

The new output matrix, $Y_{new} = (y_1\ y_2 \dots\ y_p)^T$ was computed using Equation (8).

The accuracy rate of the validation data is shown in Equation (14).

$$Accuracy\ Rate = \left(\frac{Number\ of\ validation\ data\ that\ coreectly\ classified}{Number\ of\ Validation\ data,\quad P} \times 100\% \right) \tag{14}$$

2.2.3. Prediction of the New Input Data

L, *a*, *b*, and *W* were loaded from the training phase. We loaded the new input data, $\boldsymbol{z}$, and recalculated the hidden layer matrix, $\boldsymbol{h}$, with a sigmoid activation function using Equations (12) and (13), where $\boldsymbol{w}$ is replaced with $\boldsymbol{z}$. The output, *y*, was calculated using Equation (8). Note that, based on the input data, *y* is denoted as the classified switchgear health condition.

2.3. GUI Classification

The inputs and programs of the AI development process were embedded into the GUI using the aid of Visual Basic (VB) software, to make it more user-friendly.

2.4. Data Post Processing

This is the process where the final result on the interpretation of ultrasound is shown (normal, corona, tracking, arcing, or mechanical).

3. Switchgear Data Collection

Research work was carried out to identify a multi-dimensional classification through the time and frequency domain of switchgear ultrasound data samples. Classification is to be carried out to classify the faults into a mechanical or electrical category and further analyze the pattern of the electrical faults into corona, arcing, tracking, etc. Engineers may have different interpretation from the data obtained from the measurements. Hence, the proposed intelligent solution is essential, in order to mimic the expert, avoiding unnecessary error in the decision-making. In order for the ultrasound data to be processed by MATLAB R2017a, the raw data were retrieved by using the function "audioread" and "audioinfo". The "audioread" function was used to analyze the WAVE file and the "audioinfo" function was also used to get information about the audio file. The extracted sample audio info is shown in Table 1.

Table 1. Basic information of the sample sound.

Audio File	Basic Information	Sampling Rates
Arc.wav	NumChannels: 1 SampleRate: 11,025 bit/s TotalSamples: 68,900 bits Duration: 6.2494 s BitsPerSample: 16 bps	➢ 44,100 bits per second. ➢ 22,050 bits per second. ➢ 16,000 bits per second. ➢ 11,025 bits per second (Selected as base frequency)
Corona.wav	NumChannels: 1 SampleRate: 8000 bit/s TotalSamples: 53,991 bits Duration: 6.7489 s BitsPerSample: 8 bps	
Tracking.wav	NumChannels: 1 SampleRate: 8000 bit/s TotalSamples: 52,000 bits Duration: 6.5000 s BitsPerSample: 8 bps	
Good Bearing.wav	NumChannels: 1 SampleRate: 11,025 bit/s TotalSamples: 48,551 bits Duration: 4.4037 s BitsPerSample: 16 bps	
Bad Bearing.wav	NumChannels: 1 SampleRate: 11,025 bit/s TotalSamples: 55,301 bits Duration: 5.0160 s BitsPerSample: 16 bps	

From Table 1, it can be noticed that the files comprise several sampling rates. In order to uniformly analyze and classify the ultrasound sample, the ultrasound samples in the time domain were down-converted to a uniform sampling rate, which was 11,025 bps.

In order to realign the data timeline, the higher sampling rate data need to be down-sampled. For the example, the data with a sampling rate of 44,100 bits per second is to be extracted in a multiplier of four.

After the data sampling, all the data in the time domain were collected. Then, the front part of the data needs to be truncated as highlighted and shown in Figure 4. This is due to the front part of the audio info being meaningless, as the technician just switches on the ultrasound device and not placing the device at the correct location. Besides that, the ultrasound pattern is repeated in the specific time window. Thus, the extracted data is starting from the number 1000 with a time frame of 10 Kbits (total of 10,000 as input data), as shown in Figure 5. The sample data numbers 1 to 4 in Figures 4–6 is corona, tracking, arcing, and mechanical.

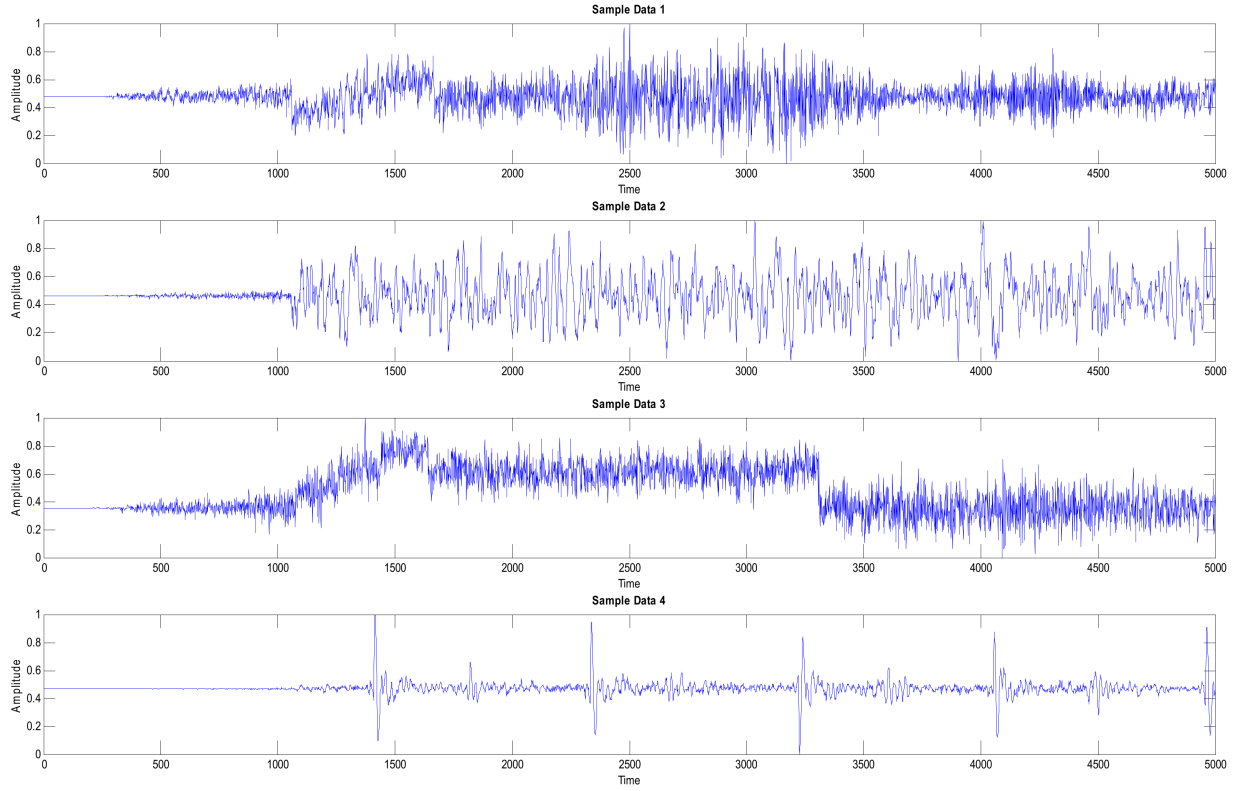

Figure 4. Time domain data extracted.

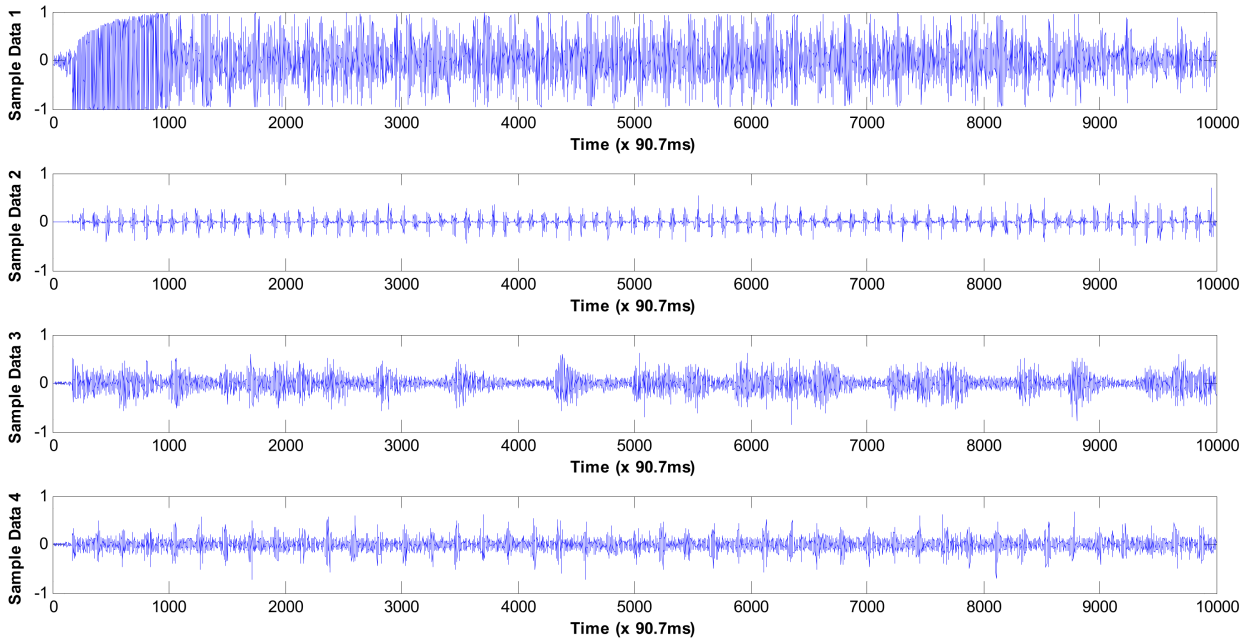

Figure 5. Final time domain data extracted.

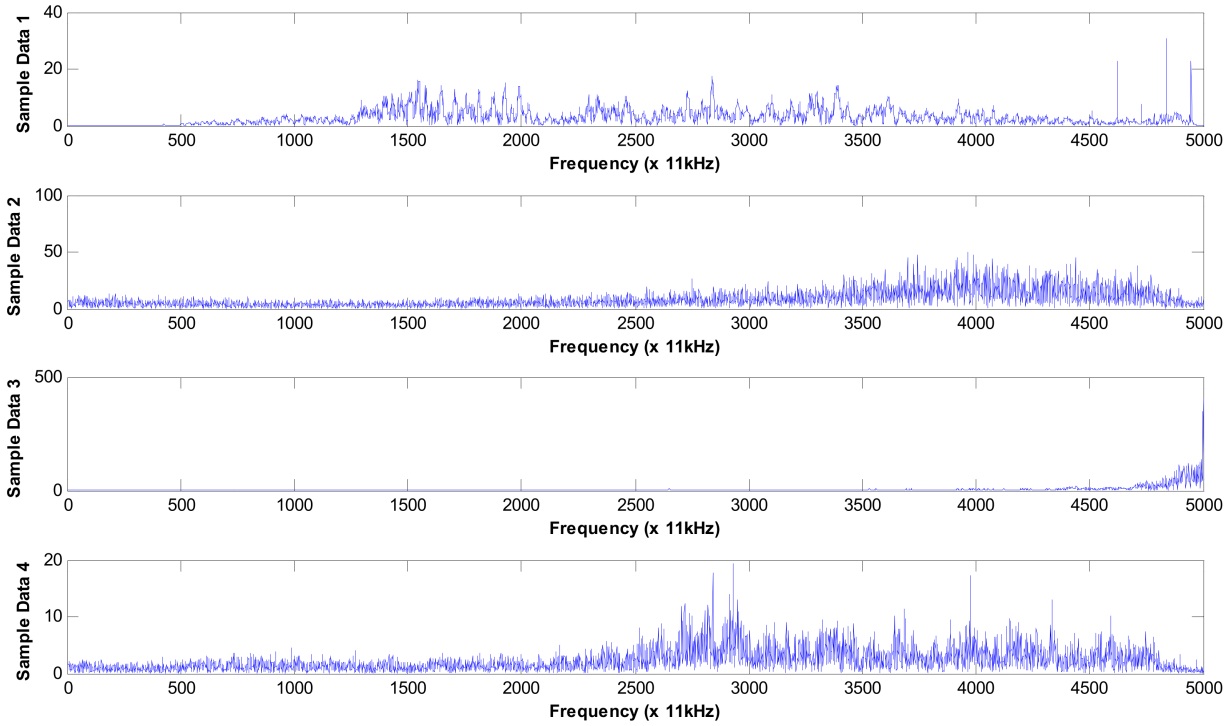

Figure 6. Frequency domain data representation.

The same process was applied for all five sets of data, which were:

- Arching—54 sets;
- Corona—41 sets;
- Mechanical—17 sets;
- Tracking—39 sets (available 314 data sets for single-channel wave file);
- Normal—13 sets.

These sets of time-domain data were then fed into the ELM for time-domain model training.

Subsequently, the fast Fourier algorithm was used to transform and map the time-domain functions into frequency-domain representations by using the one-dimensional fast Fourier transformation in MATLAB function (fft). The transformed data are shown in Figure 6.

4. Expert Rule

In order to enhance the accuracy of the classification output results, the expert rule was developed based on the time domain ultrasound amplitude, as shown in Table 2.

Table 2. The expert rule based on the time domain ultrasound amplitude.

Fault Type	Ultrasound Amplitude	
	Min	**Max**
Normal	≥ -0.015	≤ 0.015
Corona	≥ -0.2	≤ 0.2
Arching	≥ -0.8	≤ 0.8
Tracking	< -0.8	> 0.8

5. Results and Discussion

5.1. Data Pre-Processing

The list of equipment and the sampling rates are tabulated in Table 3.

Table 3. List of equipment and sampling rates.

No.	Equipment	Sampling Rate (Bits/Second)	File Format
1.	UltraTEV Plus	11,025 16,000 22,000	mp3
2.	UltraTEV Plus 2	11,025 16,000 22,000 44,100	wav
3.	Ultraprobe 9000	8000 11,025 16,000 22,000	wav
4.	Ultraprobe 10,000	8000 11,025 16,000 22,000 44,100	wav

5.2. Raw Data Collection

The total data gathered were 841 from various cases, as shown in Table 4.

Table 4. Types of faults and number of cases.

No.	Types of Faults	Cases
1.	Normal	314
2.	Corona	160
3.	Tracking	149
4.	Arcing	203
5.	Mechanical	15

5.3. Data Analysis and Correlation

The initial data were captured as a whole and required to be filtered to obtain the actual sound that reflects the actual condition by eliminating the surrounding interference. It was done by removing the first sampling. The ultrasound test results obtained previously were validated by doing an investigation at the site during the outage. Examples of the actual case studies at the PUC substation sites are shown in Table 5.

Table 5. Case studies in PUC distribution.

No.	Date	Substation	Affected Area	Finding/Remarks
1.	17 March 2018	PMU Iaduks 33 kV, Johor Bahru	Breaker compartment	Corona • Misalignment at finger arm breaker of red phase primary disconnecting switch (PDS). • Sign of embrittlement and Verdigris. • Normalized time domain amplitude = 0.2266.
2.	22 March 2018	PE Sekolah Kebangsaan Aur Atok 11 kV, Kedah	Feeder Kg Lintang, Back panel	Surface Discharge • Hair crack on the cable bushing. • Normalized time domain amplitude = 0.9375.
3.	11 March 2018	PMU Aysamet 33 kV, Selangor	Cable Compartment, Yellow phase bushing	Arcing • Sign of punctured on the bushing near to the CT. • Normalized time domain amplitude = 0.7131.

5.4. ELM Classification

ELM model development was run with the settings of the number of features, hidden nodes, and output type in corona, arcing, tracking, normal, and mechanical.

5.4.1. Corona

For corona, there were two types of domains (time domain and frequency domain) for fault classification.

Time Domain

A total of 160 data samples were used and divided into 80% training, 15% validation, and 5% testing for the classification model creation for time domain corona fault classification, as shown in Table 6. The accuracy and error rate of the classification are 87.5% and 12.5%, respectively. These results indicate that the developed ELM classification model has a high accuracy in classifying the switchgear corona fault.

Table 6. Time domain ELM classification result—corona.

Time Domain			
	Training	**Validation**	**Testing**
No Sample	128	24	8
Accuracy Rate	90.63%	87.5%	87.5%
Error Rate	9.37%	12.5%	12.5%
Feature Number		10,000	
Hidden Neuron		1200	
Output Number		1	

Corona's time domain classifier was used to classify the test datasets as either positive (P) or negative (N). This classification produces four outcomes—true positive (TP), true negative (TN), false positive (FP), and false-negative (FN), as populated in Tables 7–9—for the confusion matrix of the corona time domain classification output.

Table 7. Confusion matrix for training phase—time domain corona fault classification.

Training Phase			
		Classified Class	
		Corona	**Non-Corona**
Actual Class	Corona	26	3
	Non-Corona	9	90
Accuracy Rate		90.63%	
Error Rate		9.37%	

Table 8. Confusion matrix for validation phase—time domain corona fault classification.

Validation Phase			
		Classified Class	
		Corona	**Non-Corona**
Actual Class	Corona	1	1
	Non-Corona	2	20
Accuracy Rate		87.5%	
Error Rate		12.5%	

Table 9. Confusion matrix for testing phase—time domain corona fault classification.

Testing Phase			
		Classified Class	
		Corona	**Non-Corona**
Actual Class	Corona	1	1
	non-Corona	0	6
Accuracy Rate		87.5%	
Error Rate		12.5%	

The accuracy, *Acc*, was calculated as the total number of two correct classifications ($TP + TN$) divided by the total number of a dataset ($P + N$), which is represented in Equation (15).

$$\begin{aligned} Acc &= \frac{TP+TN}{TP+TN+FN+FP} \times 100\% \\ &= \frac{TP+TN}{P+N} \times 100\% \\ &= \frac{26+90}{29+99} \times 100\% \\ &= 90.63\% \end{aligned} \tag{15}$$

The four outcomes of a binary classifier from the training phase are as follows:
True-positive (*TP*): correct positive classification = 26;
False-positive (*FP*): incorrect positive classification = 9;
True-negative (*TN*): correct negative classification = 90;
False-negative (*FN*): incorrect negative classification 3.
The error rate (*ERR*) was calculated as the number of all incorrect classifications divided by the total number of the datasets, using Equation (16).

$$\begin{aligned} ERR &= \frac{FP+FN}{TP+TN+FN+FP} \times 100\% \\ &= \frac{FP+FN}{P+N} \times 100\% \\ &= \frac{3+9}{29+99} \times 100\% \\ &= 9.37\% \end{aligned} \tag{16}$$

The accuracy and error calculations were repeated for the validation and the testing phase, as shown in Tables 8 and 9.

Frequency Domain

A total of 160 data samples were used and divided into 80% training, 15% validation, and 5% testing for the classification model creation of the frequency domain corona fault classification, as shown in Table 10. The accuracy and error rate results of the classification are 87.5% and 12.5%, respectively. Tables 11–13 shows the confusion matrix for the training, validation, and testing phase.

Table 10. Frequency domain ELM classification result—corona.

Frequency Domain			
	Training	**Validation**	**Testing**
No Sample	128	24	8
Accuracy Rate	89.84%	83.33%	87.5%
Error Rate	10.16%	16.67%	12.5%
Feature Number		5000	
Hidden Neuron		150	
Output Number		1	

Table 11. Confusion matrix for training phase—frequency domain corona fault classification.

Training Phase			
		Classified Class	
		Corona	**Non-Corona**
Actual Class	Corona	21	3
	Non-Corona	10	94
Accuracy Rate		89.84%	
Error Rate		10.16%	

Table 12. Confusion matrix for validation phase—frequency domain corona fault classification.

Validation Phase			
		Classified Class	
		Corona	**Non-Corona**
Actual Class	Corona	3	2
	Non-Corona	2	17
Accuracy Rate		83.33%	
Error Rate		16.67%	

Table 13. Confusion matrix for testing phase—frequency domain corona fault classification.

Testing Phase			
		Classified Class	
		Corona	**Non-Corona**
Actual Class	Corona	2	0
	Non-Corona	1	5
Accuracy Rate		87.5%	
Error Rate		12.5%	

5.4.2. Summary

Tables 14 and 15 show the summary classification output of different switchgear faults (corona, arcing, tracking, normal, and mechanical). From the summary of the classification output in Tables 14 and 15, the minimum error rate was 0% and the maximum error rate was 16.67%. Meanwhile, the minimum accuracy was 83.33% and the maximum was 100%. The results show that the developed ELM classification models have a high accuracy in detecting and classifying various types of switchgear faults.

As for the output matrix for all classification faults, the accuracy for arcing and corona faults classification in the time domain was slightly lower as compared to tracking in the time domain and other faults in the frequency domain. This could be due to the cleanliness of the input data, as all the datasets provided with their labels could not be verified as valid. Among all these five classes, arcing and tracking phenomena are pretty close to each other and hence there is a possibility that the data labels done by personnel in the field for these two phenomena are not accurate.

Table 14. Summary classification output of different switchgear faults in accuracy rate.

		Accuracy Rate (%)		
		Training	**Validation**	**Testing**
ARCING	Time Domain	93.75	95.83	87.5
	Frequency Domain	93.75	91.67	100
CORONA	Time Domain	90.63	87.5	87.5
	Frequency Domain	89.84	83.33	87.5
MECHANICAL	Time Domain	96.09	91.67	100
	Frequency Domain	96.09	95.83	100
TRACKING	Time Domain	96.88	95.33	100
	Frequency Domain	96.88	91.67	100
NORMAL	Time Domain	100	95.83	100
	Frequency Domain	100	95.83	100
	Min	89.84	83.33	87.5
	max	100	95.83	100
	Average	95.391	92.449	96.25

Table 15. Summary classification output of different switchgear faults in error rate.

		Error Rate (%)		
		Training	**Validation**	**Testing**
ARCING	Time Domain	6.25	4.17	12.5
	Frequency Domain	6.25	8.33	0
CORONA	Time Domain	9.37	12.5	12.5
	Frequency Domain	10.16	16.67	12.5
MECHANICAL	Time Domain	3.91	8.33	0
	Frequency Domain	3.91	4.17	0
TRACKING	Time Domain	3.12	4.67	0
	Frequency Domain	3.12	8.33	0
NORMAL	Time Domain	0	4.17	0
	Frequency Domain	0	4.17	0
	Min	0	4.17	0
	max	10.16	16.67	12.5
	Average	4.609	7.551	3.75

To test the capability of the proposed algorithm it was compared with other approaches, as shown in Table 16. The proposed ELM is comparable (if not superior) to the other approaches.

Table 16. Benchmark compared to other approaches for diagnosing a switchgear's fault.

Approaches	Classification Accuracy Rate (%)
ELM_{ARCING}	95.83
ELM_{CORONA}	87.5
$ELM_{MECHANICAL}$	91.67
$ELM_{TRACKING}$	95.33
ELM_{NORMAL}	95.83
Random Forest [74]	87.5
Decision Tree [74]	22.9
Decision Stump [74]	50
Decision Table [74]	58.3
Multilayer Perceptron [74]	51
Optimized Feature Space—Support Vector Machine (GFS-SVM) [48]	90
Original Feature Space—Support Vector Machine (OFS-SVM) [48]	69.2
Optimized Feature Space—Random Forest (GFS-RF) [48]	86.3
Original Feature Space—Random Forest (OFS-RF) [48]	77.92
Optimized Feature Space—Density-Based Spatial Clustering of Applications with Noise (GFS-DBSCAN) [48]	98.3

6. Graphical User Interface (GUI) for Ultrasound Analyzer System (UAS)

The developed ELM model was embedded in the Visual Basic.net program. The ELM program was named the Ultrasound Analyzer System (UAS). Figure 7 is the GUI of the UAS.

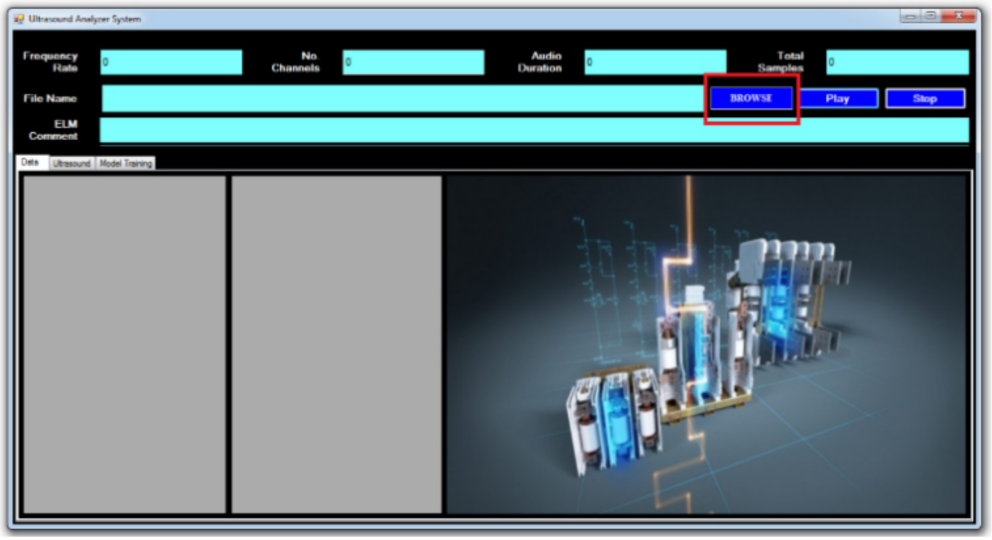

Figure 7. Ultrasound Analyzer System (UAS).

Whenever new testing data were fed into the intelligent UAS, the system determined the condition of the switchgear based on the fault severity, as shown in Table 17. The yellow box showed the result that will be selected by an intelligent ultrasound system whenever the test data meet the criteria of multiple faults.

After obtaining the ELM output result, the ELM output was combined with the expert rule output to get the final result of the intelligent UAS. The finalized result is shown in Table 18.

Table 17. Results based on severity.

Classified Results	Time-Domain				Frequency-Domain			
	Corona	**Arcing**	**Tracking**	**Mechanical**	**Corona**	**Arcing**	**Tracking**	**Mechanical**
Arcing and Mechanical	1	0	0	1	0	1	0	0
Tracking	1	1	1	0	0	1	0	0
Corona and Mechanical	1	0	0	1	1	0	0	1
Tracking	0	1	0	0	0	0	1	0
Tracking and Mechanical	1	0	1	1	1	1	0	0
Arcing	1	1	0	0	0	1	0	0

Table 18. Final output from the Ultrasound Analyzer System for a switchgear.

	ELM Output	**Expert Rule Output**	**Final Output**
Scenario 1	Normal	Any	Normal
Scenario 2	Corona	Any	Corona
Scenario 3	Tracking	Tracking	Tracking
Scenario 4	Tracking	Arcing	Arcing
Scenario 5	Arcing	Tracking	Tracking
Scenario 6	Mechanical	Any	Mechanical

7. Conclusions

This article presented the establishment of advanced data analysis procedures for switchgear mechanical fault and electrical fault identification. The data analysis and fault identification were implemented by employing an artificial intelligence algorithm, namely, Extreme Learning Machine (ELM). The analysis of the switchgear's data was carried out in two principal domains, which were the time domain and frequency domain. From the summary of the classification output in Tables 13 and 14, the minimum error rate was 0% and the maximum error rate was 16.67%. Meanwhile, the minimum accuracy was 83.33% and the maximum was 100%. The results showed that the developed ELM classification models have a high accuracy in detecting and classifying various types of switchgear faults. In addition, the ELM model for switchgear faults identification is able to provide accurate switchgear fault classification in both the time domain and in the frequency domain after the training and validation process.

The developed AI-based switchgear fault classification system was designed and incorporated with the feature of scalability and can be tested and replicated for other switchgear conditions. A customized GUI, Ultrasound Analyzer System (UAS), was also developed to enable users to obtain the switchgear condition or classification output via a graphical interface screen.

Based on the positive findings of using ELM for ultrasound analysis and switchgear fault identification, it is anticipated that the thermal image of switchgears can be useful and complement ultrasound analysis for switchgear fault identification. It is envisaged that a switchgear condition health monitoring and mitigation system can be further enhanced with thermal imaging for determining switchgear faults.

Author Contributions: Conceptualization, S.I., S.K.T. and C.P.C.; methodology, S.I., S.K.T. and C.P.C.; software, S.I., S.K.T. and C.P.C.; validation, S.I., S.K.T. and C.P.C.; formal analysis, S.I., S.K.T. and C.P.C.; investigation, S.I., S.K.T. and C.P.C.; resources, S.I., S.K.T. and C.P.C.; data curation, S.I., S.K.T. and C.P.C.; writing—original draft preparation, S.I., C.T.Y. and S.P.K.; writing—review and editing, S.I., C.T.Y., S.P.K. and T.Y.; visualization, C.T.Y. and S.P.K.; supervision, S.P.K. and S.K.T.; project administration, S.P.K., S.K.T. and C.P.C.; funding acquisition, S.P.K. All authors have read and agreed to the published version of the manuscript.

Funding: This research was funded by AAIBE Chair of Renewable Energy (ChRe), BOLD 2025 and 202101KETTHA research grant.

Institutional Review Board Statement: Not applicable.

Informed Consent Statement: Not applicable.

Data Availability Statement: Not applicable.

Acknowledgments: The authors acknowledge the use of the facilities of Universiti Tenaga Nasional Sdn. Bhd, Malaysia (UNITEN), and the AAIBE Chair of Renewable Energy (ChRe), for providing all the out-laboratory support through the BOLD 2025 and 202101KETTHA research grant.

Conflicts of Interest: The authors declare no conflict of interest.

References

1. Paoletti, G.; Blokhintsev, I.; Golubev, A. On-Line Condition Assessment of MV Electrical Switchgear and Ancillary Equipment via Partial Discharge Technology. In Proceedings of the EPRI 9th Substation Diagnostics Conference; Available online: https://www.osti.gov/biblio/835368-proceedings-substation-equipment-diagnostics-conference-ix (accessed on 29 September 2021).
2. Loo, Y.; Yaw, C.; Hashim, A.; Mohamad, A.; Faizah, M.; Noormala, A. Development of switchgear life cycle cost analysis software. In *2010 4th International Power Engineering and Optimization Conference (PEOCO)*; IEEE: New York, NY, USA, 2010; pp. 418–423. Available online: https://ieeexplore.ieee.org/abstract/document/5559217 (accessed on 29 September 2021).
3. Diessner, A.; Luxa, G.; Neyer, W. Electrical aging tests on epoxy insulators in GIS. *IEEE Trans. Electr. Insul.* **1989**, *24*, 277–283. [CrossRef]
4. Perdon, K.; Scarpellini, M.; Magoni, S.; Cavalli, L. Modular online monitoring system to allow condition-based maintenance for medium voltage switchgear. *CIRED-Open Access Proc. J.* **2017**, *1*, 346–349. [CrossRef]
5. Balobanov, R.; Zaripov, D.; Akhmadeev, A. The device for monitoring the LED display high-voltage insulators state. In *IOP Conference Series: Materials Science and Engineering*; IOP Publishing: Bristol, UK, 2019; Volume 552, no. 1, p. 012011. Available online: https://iopscience.iop.org/article/10.1088/1757-899X/552/1/012011/meta (accessed on 29 September 2021).
6. Kang, W.J.; Park, J.N.; Lee, D.H.; Shin, Y.S.; Kim, Y.K.; Oh, I.S.; Lim, K.J. Development and on-site application of UHF PD detection system to estimate the insulator condition of MV switchgear. In *2008 International Conference on Condition Monitoring and Diagnosis*; IEEE: Beijing, China, 2008; pp. 1123–1126. Available online: https://ieeexplore.ieee.org/abstract/document/4580481 (accessed on 29 September 2021).
7. Headley, P. Testing requirements for composite insulators for HV switchgear. In *IEE Colloquium on Structural Use of Composites in High Voltage Switchgear/Transmission Networks*; IET: London, UK, 1992; pp. 4/1–4/5.
8. Runde, M. Failure frequencies for high-voltage circuit breakers, disconnectors, earthing switches, instrument transformers, and gas-insulated switchgear. *IEEE Trans. Power Deliv.* **2012**, *28*, 529–530. [CrossRef]
9. Velásquez, R.M.A.; Lara, J.V.M.; Melgar, A. Reliability model for switchgear failure analysis applied to ageing. *Eng. Fail. Anal.* **2019**, *101*, 36–60. [CrossRef]
10. Shuxin, L.; Yundong, C.; Chunguang, H.; Xiaoming, L.; Jing, L. Development of on-line monitoring system of switchgear. In *2011 1st International Conference on Electric Power Equipment-Switching Technology*; IEEE: Xi'an, China, 2011; pp. 295–298. Available online: https://ieeexplore.ieee.org/abstract/document/6122992 (accessed on 29 September 2021).
11. Raju, R.; Narayananaswamy, V.; Durairaj, M.; Vittal, D.P.; Sethuraman, R.; Ananda, R.G.; Aravindakshan, A.M. Design and implementation of compact and robust medium voltage switchgear for deepwater work-class ROV ROSUB 6000. *Underw. Technol.* **2013**, *31*, 203–213. [CrossRef]
12. Chernenko, I.V. Effect of Switchgear Failures in Calculations of Structural Reliability of Power Supply Circuits at Industrial Facilities. In *2018 International Conference on Industrial Engineering, Applications and Manufacturing (ICIEAM)*; IEEE: Moscow, Russia, 2018; pp. 1–4. Available online: https://ieeexplore.ieee.org/abstract/document/8728587 (accessed on 29 September 2021).
13. Purnomoadi, A.; Mor, A.R.; Smit, J. Health index and risk assessment models for Gas Insulated Switchgear (GIS) operating under tropical conditions. *Int. J. Electr. Power Energy Syst.* **2020**, *117*, 105681. [CrossRef]
14. Boettcher, B.; Sinai, A.; Menge, M.; Gräf, T.; Plath, R.; Hücker, T. Algorithms for a Multi-Sensor Partial Discharge Expert System Applied to Medium Voltage Cable Connectors. In *2019 2nd International Conference on High Voltage Engineering and Power Systems (ICHVEPS)*; IEEE: Denpasar, Indonesia, 2019; pp. 190–195.
15. Kadechkar, A.; Moreno-Eguilaz, M.; Riba, J.-R.; Capelli, F. Low-cost online contact resistance measurement of power connectors to ease predictive maintenance. *IEEE Trans. Instrum. Meas.* **2019**, *68*, 4825–4833. [CrossRef]
16. Liu, Y.; Jia, Y.-Y.; Yang, J.-G.; Song, S.-Q.; Wu, B.; Li, J. Research of mechanical state diagnosis techniques in GIS bus connector based on mechanical vibration. In *2018 12th International Conference on the Properties and Applications of Dielectric Materials (ICPADM)*; IEEE: Xi'an, China, 2018; pp. 682–685.

17. Gauthier, J.; Sonzogni, G. The failure to break test in MV switchboards: An improvement of safety of persons and property. In Proceedings of the 1990 Third International Conference on Future Trends in Distribution Switchgear, London, UK, 23–25 April 1990; pp. 56–60.
18. Guan, X.; Qin, J.; Shu, N.; Peng, H. Studies on contact degradation process and failure mechanism of GIB plug-in connector. *IEEE Trans. Compon. Packag. Manuf. Technol.* **2019**, *9*, 1776–1784. [CrossRef]
19. Tenbohlen, S.; Denissov, D.; Hoek, S.M.; Markalous, S. Partial discharge measurement in the ultra high frequency (UHF) range. *IEEE Trans. Dielectr. Electr. Insul.* **2008**, *15*, 1544–1552. [CrossRef]
20. Uzelac, M. Test Regimes for HV and EHV Cable Connectors. In *Accessories for HV and EHV Extruded Cables: Volume 1: Components*; SpringerLinkpp: Berlin/Heidelberg, Germany, 2021; pp. 421–528.
21. Auckland, D.; McGrail, A.; Smith, C.; Varlow, B.; Zhao, J.; Zhu, D. Application of ultrasound to the inspection of insulation. *IEE Proc.-Sci. Meas. Technol.* **1996**, *143*, 177–181. [CrossRef]
22. Chen, L.-J.; Lin, W.-M.; Tsao, T.-P.; Lin, Y.-H. Study of partial discharge measurement in power equipment using acoustic technique and wavelet transform. *IEEE Trans. Power Deliv.* **2007**, *22*, 1575–1580. [CrossRef]
23. Leighton, T.G. What is ultrasound? *Prog. Biophys. Mol. Biol.* **2007**, *93*, 3–83. [CrossRef]
24. Leighton, T. Are some people suffering as a result of increasing mass exposure of the public to ultrasound in air? *Proc. R. Soc. A: Math. Phys. Eng. Sci.* **2016**, *472*, 20150624. [CrossRef]
25. Maher, R.C. *Principles of Forensic Audio Analysis*; Springer: Berlin/Heidelberg, Germany, 2018; Available online: https://link.springer.com/book/10.1007%2F978-3-319-99453-6 (accessed on 29 September 2021).
26. Soliman, M.H.A. Ultrasound Analysis for Condition Monitoring: Applications of Ultrasound Detection for Various Industrial Equipment. Mohammed Hamed Ahmed Soliman: Berlin/Heidelberg, Germany, 2020. Available online: https://books.google.com.my/books?hl=en&lr=&id=oM4uEAAAQBAJ&oi=fnd&pg=PA3&dq=Ultrasound+Analysis+for+Condition+Monitoring:+Applications+of+Ultrasound+Detection+for+Various+Industrial+Equipment&ots=LHKcKaTnK-&sig=unKxM3VZp0BRImSrJKK_uv7RJck&redir_esc=y#v=onepage&q=Ultrasound%20Analysis%20for%20Condition%20Monitoring%3A%20Applications%20of%20Ultrasound%20Detection%20for%20Various%20Industrial%20Equipment&f=false (accessed on 29 September 2021).
27. Brady, J.; Thermographer, L.-I.C. *Corona and Tracking Conditions in Metal-Clad Switchgear Case Studies*; Brady Infrared Insp: Stuart, FL, USA, 2006.
28. Javed, H.; Kang, L.; Zhang, G. The Study of Different Metals Effect on Ozone Generation Under Corona Discharge in MV Switchgear Used for Fault Diagnostic. In Proceedings of the 2019 IEEE Asia Power and Energy Engineering Conference (APEEC), Chengdu, China, 29–31 March 2019; pp. 29–33.
29. Weichert, H.; Benz, P.; Hill, N.; Hilbert, M.; Kurrat, M. On Partial Discharge/Corona Considerations for Low Voltage Switchgear and Controlgear. In *2018 IEEE Holm Conference on Electrical Contacts*; IEEE: Albuquerque, NM, USA, 2018; pp. 246–253.
30. Ishak, S.; Koh, S.-P.; Tan, J.-D.; Tiong, S.-K.; Chen, C.-P. Corona fault detection in switchgear with extreme learning machine. *Bull. Electr. Eng. Inform.* **2020**, *9*, 558–564. [CrossRef]
31. Tang, J.; Liu, F.; Zhang, X.; Ren, X.; Fan, M. Characteristics of the Concentration Ratio of SO_2F_2 to SOF_2 as the Decomposition Products of SF_6 Under Corona Discharge. *IEEE Trans. Plasma Sci.* **2011**, *40*, 56–62. [CrossRef]
32. Raj, A.; Ishak, S.; Amir, M.; Yogendra, B.; Raffi, M. Corona Detection Using Wide Band Antenna and Time Delay Method. *Telkomnika* **2017**, *15*, 1547–1553. [CrossRef]
33. Cho, H.-S. Frequency Spectrum Analysis of Corona Discharge Source Measured by Ultrasound Detector. *J. Korea Inst. Inf. Electron. Commun. Technol.* **2019**, *12*, 78–82.
34. Chidurala, M. Electrical Equipment Reliability with Ultrasound. *Water Energy Int.* **2016**, *59*, 16–18.
35. Haiguo, T.; Jiran, Z.; Fangliang, G.; Hua, L.; Min, F.; Qi, H. Research on a rail-robot based remote three-dimensional inspection system for switch stations in power distribution network. In Proceedings of the 2017 Chinese Automation Congress (CAC), Jinan, Xian, 20–22 October 2017; pp. 7925–7930.
36. Baug, A.; Choudhury, N.R.; Ghosh, R.; Dalai, S.; Chatterjee, B. Identification of single and multiple partial discharge sources by optical method using mathematical morphology aided sparse representation classifier. *IEEE Trans. Dielectr. Electr. Insul.* **2017**, *24*, 3703–3712. [CrossRef]
37. Hussain, G.A.; Kumpulainen, L.; Klüss, J.V.; Lehtonen, M.; Kay, J.A. The smart solution for the prediction of slowly developing electrical faults in MV switchgear using partial discharge measurements. *IEEE Trans. Power Deliv.* **2013**, *28*, 2309–2316. [CrossRef]
38. Paoletti, G.; Baier, M. Failure contributors of MV electrical equipment and condition assessment program development. In Proceedings of the Conference Record of 2001 Annual Pulp and Paper Industry Technical Conference (Cat. No. 01CH37209), Portland, OR, USA, 18–22 June 2001; pp. 37–47.
39. Tahan, M.; Muhammad, M.; Karim, Z.A. A framework for intelligent condition-based maintenance of rotating equipment using mechanical condition monitoring. In Proceedings of the MATEC Web of Conferences, Pilsen, Czech Republic, 7–9 September 2021; p. 05011.
40. Hwang, H.; Lee, J.; Hwang, J.; Jun, H. A study of the development of a condition-based maintenance system for an LNG FPSO. *Ocean Eng.* **2018**, *164*, 604–615. [CrossRef]
41. Vogl, G.W.; Weiss, B.A.; Helu, M. A review of diagnostic and prognostic capabilities and best practices for manufacturing. *J. Intell. Manuf.* **2019**, *30*, 79–95. [CrossRef]

42. Goyal, D.; Pabla, B.; Dhami, S.; Lachhwani, K. Optimization of condition-based maintenance using soft computing. *Neural Comput. Appl.* **2017**, *28*, 829–844. [CrossRef]
43. Tahan, M.; Tsoutsanis, E.; Muhammad, M.; Karim, Z.A. Performance-based health monitoring, diagnostics and prognostics for condition-based maintenance of gas turbines: A review. *Appl. Energy* **2017**, *198*, 122–144. [CrossRef]
44. Hoffmann, M.W.; Wildermuth, S.; Gitzel, R.; Boyaci, A.; Gebhardt, J.; Kaul, H.; Amihai, I.; Forg, B.; Suriyah, M.; Leibfried, T. Integration of novel sensors and machine learning for predictive maintenance in medium voltage switchgear to enable the energy and mobility revolutions. *Sensors* **2020**, *20*, 2099. [CrossRef] [PubMed]
45. Zheng, K.; Si, G.; Diao, L.; Zhou, Z.; Chen, J.; Yue, W. Applications of support vector machine and improved k-Nearest Neighbor algorithm in fault diagnosis and fault degree evaluation of gas insulated switchgear. In Proceedings of the 2017 1st International Conference on Electrical Materials and Power Equipment (ICEMPE), Xian, China, 14–17 May 2017; pp. 364–368.
46. Nguyen, M.-T.; Nguyen, V.-H.; Yun, S.-J.; Kim, Y.-H. Recurrent neural network for partial discharge diagnosis in gas-insulated switchgear. *Energies* **2018**, *11*, 1202. [CrossRef]
47. Wang, Y.; Yan, J.; Yang, Z.; Liu, T.; Zhao, Y.; Li, J. Partial discharge pattern recognition of gas-insulated switchgear via a light-scale convolutional neural network. *Energies* **2019**, *12*, 4674. [CrossRef]
48. Yuan, Y.; Ma, S.; Wu, J.; Jia, B.; Li, W.; Luo, X. Fault diagnosis in gas insulated switchgear based on genetic algorithm and density-based spatial clustering of applications with noise. *IEEE Sens. J.* **2019**, *21*, 965–973. [CrossRef]
49. Gong, Y.; Liu, Y.; Wu, L. Identification of partial discharge in gas insulated switchgears with fractal theory and support vector machine. *Power Syst. Technol.* **2011**, *35*, 135–139.
50. Wang, Y.; Yan, J.; Jing, Q.; Qi, Z.; Wang, J.; Geng, Y. A novel adversarial transfer learning in deep convolutional neural network for intelligent diagnosis of gas-insulated switchgear insulation defect: A DATCNN for GIS insulation defect diagnosis. *IET Gener. Trans. Distrib.* **2021**. [CrossRef]
51. Sukma, T.R.; Khayam, U.; Sugawara, R.; Yoshikawa, H.; Kozako, M.; Hikita, M.; Eda, O.; Otsuka, M.; Kaneko, H.; Shiina, Y. Determination of type of partial discharge in cubicle-type gas insulated switchgear (C-GIS) using artificial neural network. In Proceedings of the 2018 Condition Monitoring and Diagnosis (CMD), Perth, Western Australia, 23–26 September 2018; pp. 1–5.
52. Zhiwei, L.; Kehui, Z.; Xiaochun, Z. Research on Fault Diagnosis of Switchgear Contacts Based on BP Neural Network. In Proceedings of the 2018 International Conference on Power System Technology (POWERCON), Guangzhou, China, 6–9 November 2018; pp. 3507–3513.
53. Barrios, S.; Buldain, D.; Comech, M.P.; Gilbert, I. Partial Discharge Identification in MV switchgear using Scalogram representations and Convolutional AutoEncoder. *IEEE Trans. Power Deliv.* **2020**. Available online: https://ieeexplore.ieee.org/abstract/document/9286573 (accessed on 29 September 2021). [CrossRef]
54. Tuyet-Doan, V.-N.; Pho, H.-A.; Lee, B.; Kim, Y.-H. Deep Ensemble Model for Unknown Partial Discharge Diagnosis in Gas-Insulated Switchgears Using Convolutional Neural Networks. *IEEE Access* **2021**, *9*, 80524–80534. [CrossRef]
55. Zhang, J.-M.; Yin, J.-H.; Jiang, X.-X. Application of RBF network-based state assessment technique of high voltage switchgear to intelligent GIS. *High Volt. Appar.* **2013**, *49*, 115–121.
56. Xue, W. Improved method of high voltage switchgear temperature prediction based on WNN. *Appl. Mech. Mater.* **2014**, *644–650*, 502–505. Available online: https://www.scientific.net/AMM.644-650.502 (accessed on 29 September 2021). [CrossRef]
57. Feng, X.; Zhou, Y.; Hua, T.; Zou, Y.; Xiao, J. Contact temperature prediction of high voltage switchgear based on multiple linear regression model. In Proceedings of the 2017 32nd Youth Academic Annual Conference of Chinese Association of Automation (YAC), Hefei, China, 19–21 May 2018; pp. 277–280.
58. Qiao, X.; Gao, K.; Huang, H.; Lyu, L.; Lin, W.; Jin, L. Temperature Rise Prediction of GIS Electrical Contact Using an Improved Kalman Filter. In Proceedings of the IECON 2019–45th Annual Conference of the IEEE Industrial Electronics Society, Lisbon, Portugal, 14–17 September 2019; pp. 167–172.
59. Huang, G.-B.; Wang, D.H.; Lan, Y. Extreme learning machines: A survey. *Int. J. Mach. Learn. Cybern.* **2011**, *2*, 107–122. [CrossRef]
60. Huang, G.; Huang, G.-B.; Song, S.; You, K. Trends in extreme learning machines: A review. *Neural Netw.* **2015**, *61*, 32–48. [CrossRef] [PubMed]
61. Huang, G.; Song, S.; Gupta, J.N.; Wu, C. Semi-supervised and unsupervised extreme learning machines. *IEEE Trans. Cybern.* **2014**, *44*, 2405–2417. [CrossRef]
62. Deng, C.; Huang, G.; Xu, J.; Tang, J. Extreme learning machines: New trends and applications. *Sci. China Inf. Sci.* **2015**, *58*, 1–16. [CrossRef]
63. Huang, G.-B. An insight into extreme learning machines: Random neurons, random features and kernels. *Cogn. Comput.* **2014**, *6*, 376–390. [CrossRef]
64. Yaw, C.T.; Yap, K.S.; Wong, S.Y.; Yap, H.J.; Paw, J.K.S. Enhancement of Neural Network Based Multi Agent System for Classification and Regression in Energy System. *IEEE Access* **2020**, *8*, 163026–163043. [CrossRef]
65. Yadav, B.; Ch, S.; Mathur, S.; Adamowski, J. Assessing the suitability of extreme learning machines (ELM) for groundwater level prediction. *J. Water Land Dev.* **2017**, 103–112. [CrossRef]
66. Bartlett, P.L. The sample complexity of pattern classification with neural networks: The size of the weights is more important than the size of the network. *IEEE Trans. Inf. Theory* **1998**, *44*, 525–536. [CrossRef]

67. Huang, G.-B.; Zhu, Q.-Y.; Siew, C.-K. Extreme learning machine: A new learning scheme of feedforward neural networks. In Proceedings of the 2004 IEEE International Joint Conference on Neural Networks (IEEE Cat. No. 04CH37541), Budapest, Hungary, 25–29 July 2004; pp. 985–990.
68. Pacheco, A.G.; Krohling, R.A.; da Silva, C.A. Restricted Boltzmann machine to determine the input weights for extreme learning machines. *Expert Syst. Appl.* **2018**, *96*, 77–85. [CrossRef]
69. Yaw, C.T.; Wong, S.Y.; Yap, K.S.; Yap, H.J.; Amirulddin, U.A.U.; Tan, S.C. An ELM based multi-agent system and its applications to power generation. *Intell. Decis. Technol.* **2018**, *12*, 163–171. [CrossRef]
70. Luo, M.; Zhang, K. A hybrid approach combining extreme learning machine and sparse representation for image classification. *Eng. Appl. Artif. Intell.* **2014**, *27*, 228–235. [CrossRef]
71. Lu, S.; Wang, X.; Zhang, G.; Zhou, X. Effective algorithms of the Moore-Penrose inverse matrices for extreme learning machine. *Intell. Data Anal.* **2015**, *19*, 743–760. [CrossRef]
72. Tang, J.; Deng, C.; Huang, G.-B. Extreme learning machine for multilayer perceptron. *IEEE Trans. Neural Netw. Learn. Syst.* **2015**, *27*, 809–821. [CrossRef]
73. Huang, G.-B.; Zhu, Q.-Y.; Siew, C.-K. Extreme learning machine: Theory and applications. *Neurocomputing* **2006**, *70*, 489–501. [CrossRef]
74. Muhamad, N.A.; Musa, I.V.; Malek, Z.A.; Mahdi, A.S. Classification of Partial Discharge Fault Sources on SF^6 Insulated Switchgear Based on Twelve By-Product Gases Random Forest Pattern Recognition. *IEEE Access* **2020**, *8*, 212659–212674. [CrossRef]